

Directly Probing Effective-Mass Anisotropy of Two-Dimensional ReSe₂ in Schottky Tunnel Transistors

Xiaochi Liu,¹ Yahua Yuan,¹ Zhongwang Wang,¹ Russell S. Deacon,^{2,3} Won Jong Yoo,⁴ Jian Sun,^{1,2,*} and Koji Ishibashi^{2,3}

¹School of Physics and Electronics, Central South University, 932 South Lushan Road, Changsha 410083, China

²Advanced Device Laboratory, RIKEN, 2-1 Hirosawa, Wako, Saitama 351-0198, Japan

³Center for Emergent Matter Science, RIKEN, 2-1 Hirosawa, Wako, Saitama 351-0198, Japan

⁴SKKU Advanced Institute of Nano-Technology (SAINT), Sungkyunkwan University, 2066 Seobu-ro, Suwon, Gyeonggi-do 16419, Republic of Korea



(Received 23 February 2020; accepted 1 April 2020; published 22 April 2020)

Anisotropic physical properties in two-dimensional (2D) layered semiconductors with low crystal lattice symmetry are of great interest due to the underlying rich physics and potential applications in electronics. Sophisticated transport measurements unveiling the anisotropic effective mass, which is an essential material parameter reflecting the energy band, are still lacking so far. With a focus on the anisotropy with respect to the underlying crystal structure, in this work, we propose a simple strategy to directly probe the carrier effective mass m^* for 2D semiconductors using tunneling as the sensing tool. The Schottky tunnel transistor is a practically simple device, in which the transport can be electrically tuned to be tunneling dominated. Using such a device as the experimental platform, we extract the anisotropy of the effective mass for both electrons and holes in the low symmetric ReSe₂ from the Fowler-Nordheim tunneling measured at 1.4 K. Furthermore, a colossal conductivity anisotropy of 10³ is observed for ReSe₂.

DOI: 10.1103/PhysRevApplied.13.044056

I. INTRODUCTION

Two-dimensional (2D) layered semiconductors with low crystal lattice symmetry, such as black phosphorus and rhenium dichalcogenides, possess intrinsic in-plane anisotropic physical properties [1–3], which permit unique applications, such as polarization-sensitive photodetectors and anisotropic FETs [4–6]. ReSe₂ is a typical 2D semiconductor with notable anisotropy, which has a layered triclinic structure with lattice symmetry of group $P\bar{1}$ as illustrated in Fig. 1(a) [7]. The rhenium atoms are sandwiched between selenium atoms forming a monolayer and these layers stack along the crystallographic c axis at an oblique angle to the basal layers. Owing to the Peierls distortion, adjacent rhenium atoms are bonded into the four-atom “lozenge” clusters to form the Re chains along the a axis, resulting in the unique properties different from other crystallographic axes. Additionally, ReSe₂ is stable in ambient condition, making it easy to handle in processing and thus an ideal material platform to study anisotropy.

The photoluminescence emission and polarized Raman spectroscopy are the commonly utilized tools to investigate the anisotropy of 2D semiconductors [10,11]. So far the reported transport measurements are mainly focused

on the anisotropic conductivity or field-effect mobility in 2D materials. For instance, the conductivity anisotropy with a ratio of approximately 10 has been reported for ReS₂, an isostructural crystal to ReSe₂ [12]. By contrast, the effective mass m^* is a more essential material parameter. The anisotropy of m^* reflecting the shape of the energy band is of great importance for designing high-performance transistors with very scaled-down channels or tunneling devices. A twofold asymmetric distribution of effective hole mass near its VBM has been discovered for ReSe₂ with its minimum (maximum) along (normal to) the a axis by directly measuring its energy band structure using angle-resolved photoemission spectroscopy (ARPES) [13]. Nevertheless, ARPES measurement has a relatively low resolution in terms of energy and it is technically challenging especially for the samples with submicron dimensions [14]. Sophisticated transport measurements to directly probe the anisotropic m^* and the electronic band structure are lacking. Effective mass and its anisotropy can be extracted from the temperature dependence of the quantum oscillations measured in a magnetic field [15]. However, under a limited magnetic field B , this only applies to those systems with high carrier mobility $\mu \gg 1/B$. Hence, we are encouraged to explore a universal method to directly measure the anisotropy of the effective mass near VBM or conduction-band minimum (CBM) in

*jian.sun@csu.edu.cn

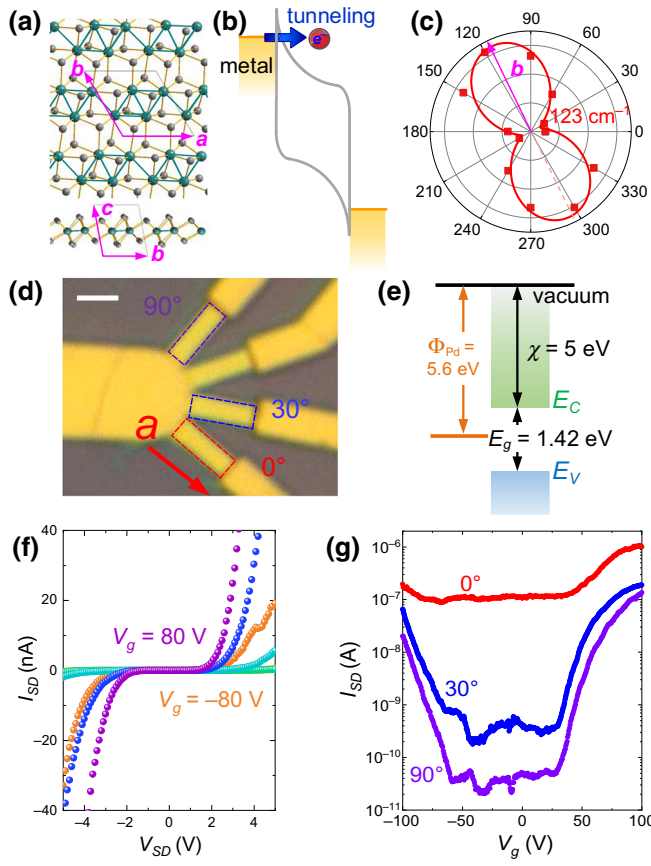


FIG. 1. (a) Crystal structure of ReSe_2 . The a axis is along the rhenium chain. (b) Band diagram showing the tunneling via the triangle-shape barrier formed in a Schottky transistor at a dc bias. (c) Peak intensity of the 123 cm^{-1} mode of ReSe_2 as a function of the excitation polarization direction with its maximum aligning to the b axis. The symbols represent experimental data while the solid curve is the fit from Raman analysis. (d) Micrograph of the as-fabricated ReSe_2 transistors with their channel orientations rotated by θ from the a axis. Dashed boxes highlight the ReSe_2 ribbons. Scale bar: $1 \mu\text{m}$. (e) Band alignment of the palladium contact and ReSe_2 . ReSe_2 has an electron affinity χ of 5 eV and a band gap E_g of 1.42 eV [8]. Palladium contact has a work function Φ_{Pd} of 5.6 eV [9]. (f) Output curves of ReSe_2 FET in 30° orientation measured at 1.4 K at varied gate voltages. (g) Anisotropic transfer characteristics measured in the Schottky transistors along varied orientations at a high bias of 5 V .

2D semiconductors via the simple and feasible transport measurement.

In addition, we know that the tunneling of either electron or hole through a triangle-shape barrier, i.e., Fowler-Nordheim (FN) tunneling, is correlated to the effective mass of the material. The tunneling current into a semiconductor with relatively low band gap can be expressed by a simplified equation with the parabolic WKB approximation [16,17],

$$I_{SD} \propto V_{SD}^2 \times e^{(-8\pi d\sqrt{2m^*}\phi_B^{3/2})/3heV_{SD}}, \quad (1)$$

where h is Planck's constant, e is electron charge, and d and ϕ_B are the width and height of the Schottky barrier, respectively. By measuring the FN tunneling through the identical barriers built in the material along different orientations, the anisotropy of the effective mass can be simply extracted. In practice, Schottky FETs with short channels are considered as one of the ideal device platforms to host FN tunneling from metal contact to the CBM (VBM) of a semiconductor. Compared to a lateral tunnel junction, which requires accurate doping profile or complex device architecture with fine gates [18], Schottky FETs can be easily obtained with an ordinary FET geometry. The triangle-shape Schottky barriers are naturally formed at the contact interfaces due to the band bending by choosing appropriate metal contacts [Fig. 1(b)] [19]. Furthermore, the so-called drain-induced barrier lowering (DIBL) [20], which is very pronounced in a short channel transistor, can be employed to electrically set the optimal Schottky barrier width to allow FN tunneling.

Here we report a direct transport measurement of the anisotropy of effective mass for ReSe_2 in the tunneling dominated Schottky transistors. The electrically tunable triangle-shape Schottky barrier is set by choosing the contact metal and applying the thermal annealing. A colossal tunneling conductivity anisotropy of 10^3 is measured in the ReSe_2 with strong gate tunability. The information of the effective mass m^* is extracted from the measured tunneling conductivity. Our measurements reveal the strongly anisotropic effective-mass distribution for the ReSe_2 layer, with the lightest carriers being along its a axis and the heaviest hole and electron residing in the orientation normal to its a axis. This method provides a considerably high accuracy, showing a good agreement with the previously reported ARPES data.

II. RESULTS AND DISCUSSION

We firstly show polarized Raman spectroscopy measurements on the exfoliated ReSe_2 thin flakes, which carries information on phonon modes associated with the lattice symmetry. Figure 1(c) plots the peak intensity of a typical Raman mode at 123 cm^{-1} with respect to the laser polarization. A twofold symmetry is noted and is consistent with previous reports [21]. The peak intensity is known to exhibit its maximum along the b axis with an inner angle of approximately 120° to a . Subsequently, taking the polarized Raman spectrum as the reference, we can determine the crystal orientation for a ReSe_2 flake without knowing its crystalline structure. The ReSe_2 used for the transport measurements are fabricated along the varied crystal orientations with palladium contacts (see details within the Supplemental Material [22]). Dry-etching-defined ribbon-shape channels of $1.5 \mu\text{m}$ length and $0.5 \mu\text{m}$ width are employed to fully confine the transport in the desired orientation. Figure 1(d) shows three

fabricated devices from one approximately 10-nm-thick ReSe_2 flake with the channels orientating in varied θ of 0° , 30° , and 90° rotated from the a axis. Note the device with the ribbon along 60° is not measured due to a broken contact after fabrication. The information of 60° is obtained in an additional device, which is presented in the Supplemental Material [22]. Palladium has its work function approximately in the middle of the ReSe_2 band gap as illustrated in Fig. 1(e). We therefore anticipate ambipolar transport, which allows us to investigate both electron and hole transport. A thermal annealing after fabrication is necessary to set the optimal Schottky contact (for details see the Supplemental Material [22]).

In such a device, the initial Schottky barrier, which is defined as the energy gap between the Fermi level of metal and conduction- (valence-) band minimum (maximum) of ReSe_2 , is estimated to be as large as 0.6 eV for electrons and 0.8 eV for holes, respectively [23]. Hence, the transport is impeded and no current is observed in the output curve at the low dc bias as shown in Fig. 1(f). At the high bias of >2 V, current starts to increase and nano ampere signals can be measured. Figure 1(g) plots the transfer characteristics of these three transistors at a high dc bias of 5 V at 1.4 K. As expected, the ambipolar transport is achieved in all devices with the clear *off* state appearing in an identical gate voltage range from -60 to 40 V, which highlights the good device uniformity in one fabrication batch. More interestingly, as channel orientation changes from 0° (a axis) to 90° , the drain current I_{SD} decreases dramatically. Since the device parameters are identical in these transistors, this discrepancy strongly suggests an anisotropy residing in the a - b plane. The high leakage current in the *off* state along 0° and 30° FETs manifests that these FETs cannot be fully switched off, possibly indicating the presence of short channel. However, before using Eq. (1) to extract the information for effective mass, we verify that transport is dominated by tunneling.

Two mechanisms, tunneling and thermionic emission, contribute to the transport in a Schottky transistor [24], as illustrated in the inset of Fig. 2(a). In our experiment, the thermionic emission is heavily suppressed by carrying

out the measurements at a low temperature of 1.4 K. Figures 2(a) and 2(b) plot the transfer characteristics and output curves measured in the transistors along 90° at 1.4 and 150 K, respectively. Considering the contact-limited transport in this Schottky transistor, the contribution of the channel can be negligible. Therefore, the temperature dependence of the measured current basically originates from the changes of the contacts when varying temperature. Currents I_{SD} in both *off* and *on* states of the gate modulation are significantly enhanced at 150 K, suggesting the existence of the temperature-enabled transport, i.e., thermionic emission. Additionally, the output curves show a dramatic increase of I_{SD} by a few orders at the low bias of approximately 1 V at 150 K. The slight asymmetry of the output curves under forward and reverse drain biases is ascribed to the different heights of the image force barrier reduction at two contacts [25]. When thermionic emission is dominant, $\ln(I_{SD})$ exhibits a linear correlation between $\sqrt{V_{SD}}$ and vice versa [26]. We replot the output curves in the form of $\ln(I_{SD})$ vs $\sqrt{V_{SD}}$ in Fig. 2(c). The data measured at 150 K can be well fitted to linear lines at bias of >1 V. In contrast, the poor linearity of the data at 1.4 K suggests that the thermionic emission is excluded from the possible transport mechanism at low temperature. The effective Schottky barrier ϕ_B at high dc bias can be estimated from the temperature dependence of the *on* state current of the Schottky transistor using the thermionic emission equation [24]

$$I_{SD} \propto T^{3/2} \times e^{\left(\frac{-q\phi_B^{3/2}}{k_B T} \right)}, \quad (2)$$

with q and k_B being electron charge and Boltzmann constant, respectively. The transfer characteristics measured in an approximately 5-nm-thick ReSe_2 at the varied temperatures with $V_{SD} = 5$ V are plotted in the Supplemental Material [22]. The low ϕ_B in the order of 10 meV is extracted for the electron branch by fitting Eq. (2) to the data from $V_g = 60$ to 80 V, which is in a reasonable regime for the obtained current level hosted by tunneling.

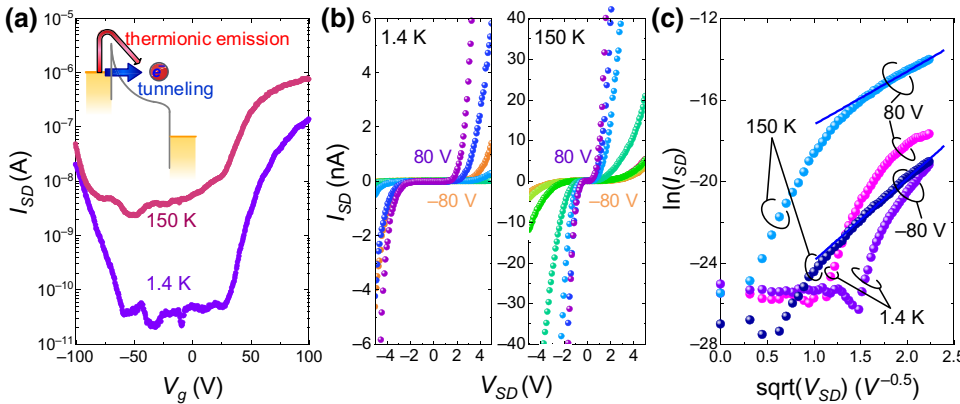


FIG. 2. (a),(b) Transfer characteristics and output curves of the ReSe_2 FET in the 90° orientation at 1.4 and 150 K, respectively. Inset of (a), the band diagram illustrating two carrier transport mechanisms. (c) Plots of thermionic emission fitting under gate voltages of ± 80 V at 1.4 and 150 K. Solid lines are the linear fits to the data at 150 K at V_{SD} from 1 to 5 V.

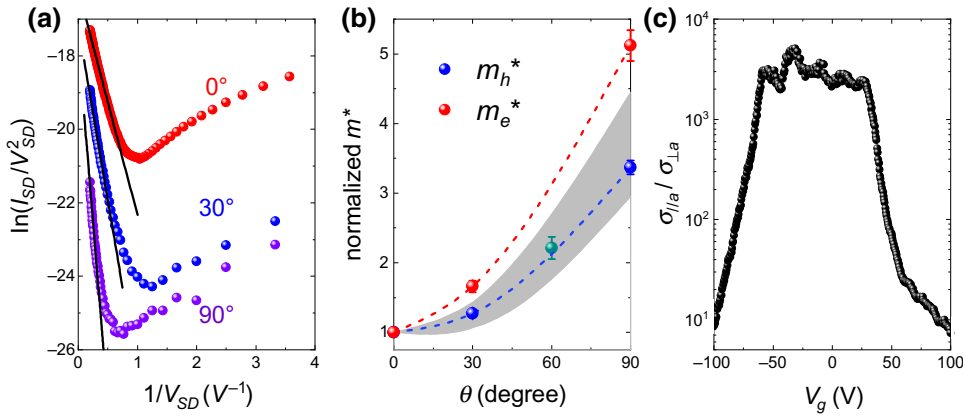


FIG. 3. (a) Output data measured in varied orientations at $V_g = 80$ V. Solid lines are the linear fits to the FN tunneling model using Eq. (2). (b) Extraction of the normalized effective electron mass m_e^* and hole mass m_h^* to 0° for varied orientations. The green dot plots the normalized hole effective mass along 60° extracted from an additional device by comparing to 90° (Fig. S1 within the Supplemental Material [22]). The gray shadow indicates to the effective normalized hole mass m_h^* measured by ARPES [13]. (c) Colossal in-plane conductivity anisotropy in the ReSe_2 Schottky FETs.

Considering the high ϕ_B of 10^2 meV of the intrinsic barrier, the excellence of the DIBL effect for modulating the Schottky barrier is highlighted.

In the tunneling transport, the linear correlation between $\ln(I_{SD}/V_{SD}^2)$ and $1/V_{SD}$ is derived from Eq. (1) [27]. Hence in Fig. 3(a) we plot the output data measured along 0° , 30° , and 90° at 1.4 K under $V_g = 80$ V in the form of $\ln(I_{SD}/V_{SD}^2)$ vs $1/V_{SD}$, respectively. The good linear fits to the high-bias regime give solid evidence for dominant FN tunneling transport and eliminate the possibility of considerable current contributions from other tunneling mechanisms, for instance trap-assisted tunneling via the defective states inside the barrier. In addition, knowing that there is no other energy band or state having the similar energy near the CBM or VBM in ReSe_2 , the tunneling is anticipated mainly occurring from the contacts to the CBM or VBM. Furthermore, considering the facts, such as low defect density in the mechanically exfoliated flake from the high-quality crystal, well-optimized contact interface in the Schottky transistor, small thermal energy of approximately 0.1 meV at a measurement temperature of 1.4 K, the inelastic scattering processes due to defects or associated with phonon are very unlikely to take place. Conservation of momentum and energy is satisfied in the FN-tunneling process. We are now confident to quantitatively extract the effective-mass anisotropy near the CBM and VBM using Eq. (1). The effective mass is calculated as

$$m^* \propto \left[1/d \times \phi_B^{-3/2} \times \frac{d\ln(I_{SD}/V_{SD}^2)}{d(1/V_{SD})} \right]^2, \quad (3)$$

where $d\ln(I_{SD}/V_{SD}^2)/d(1/V_{SD})$ presents the slope of the linear regime. The fitted lines get steeper as θ increases from 0° to 90° , therefore implying heavier m^* . The nearly identical contacts are expected from the well-controlled

fabrication. Therefore, d and ϕ_B are expected to be constants in all devices made on the same ReSe_2 flake in the same fabrication batch. To investigate the anisotropy of effective masses, we find that it is not necessary to analytically describe the tunneling and quantitatively obtain the exact values of m^* by employing a complex analytical model. Instead, the information of m^* anisotropy can be simply and precisely extracted for both electron and hole without knowing the exact value of d and ϕ_B by normalizing m^* with that at 0° . The results are plotted in Fig. 3(b) with respect to θ . Both m_e^* and m_h^* increase with the deviation from 0° (a axis). The anisotropy between a axis and $\perp a$ axis is as high as 3.4 and 5.1 for m_h^* and m_e^* , reflecting the asymmetric energy band near VBM and CBM, respectively. The extracted anisotropy of effective hole mass m_h^* resembles the one measured by ARPES at the VBM, which is marked by the gray shadow in Fig. 3(b) [13]. This verifies that the m^* anisotropies we obtain are mainly probed at the VBM and CBM as anticipated. It is known that m^* changes with energy. Noted that this energy dependence of effective mass as well as its impact on anisotropy are not considered in this work. Additionally, we notice that the normalized m_h^* for 60° extracted in a different device falls within this reasonable range, highlighting the reproducibility of the proposed method. As a result, the colossal conductivity anisotropy, which is defined as the ratio between the conductivity σ in 0° ($\parallel a$) and 90° ($\perp a$), is observed in the ReSe_2 with Schottky tunnel transistors [Fig. 3(c)]. A maximum $\sigma_{\parallel a}/\sigma_{\perp a}$ of approximately 4000 is noted in association with the *off* state of the transistor. To our knowledge, this value is the highest among all 2D transition metal dichalcogenides and on a par with that recently reported anisotropy for gallium telluride [28].

Finally, we discuss the colossal conductivity anisotropy by showing the DIBL effect and its distinct impact on the

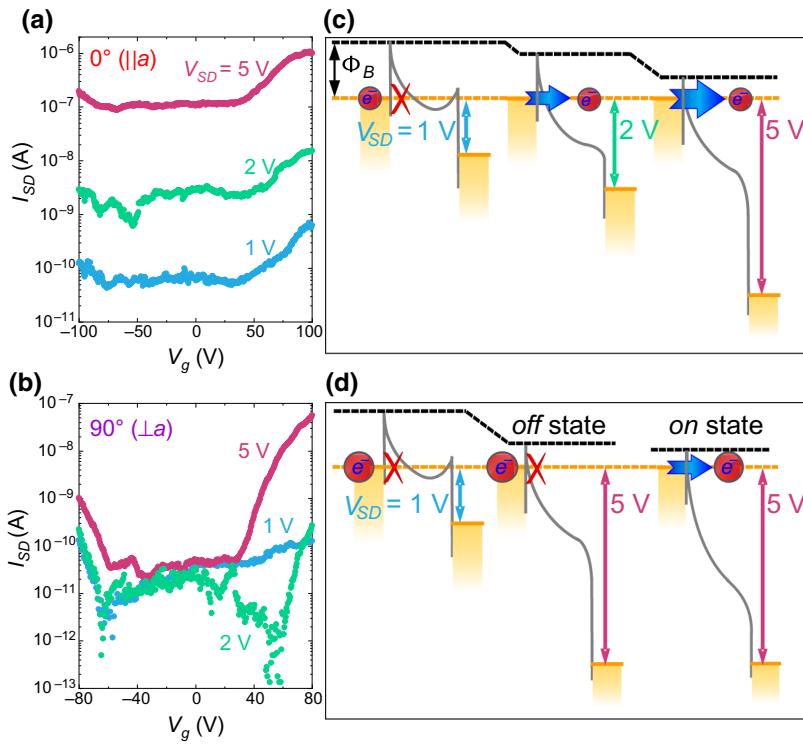


FIG. 4. (a),(b) Transfer characteristics of the ReSe₂ Schottky transistor in $\parallel a$ axis (along the rhenium chain) and 90° axis (perpendicular to the rhenium chain) under varied drain biases. Band diagram showing (c) the transport via the Pd-ReSe₂ Schottky barrier in the $\parallel a$ axis under varied drain biases in the *off* state, and (d) the transport in the 90° axis under varied drain biases in both the *off* state and the *on* state.

transport in the biased Schottky transistors due to the m^* anisotropy along varied orientations. The transfer characteristics of the Schottky transistor oriented in 0° and 90° at varied dc bias V_{SD} are plotted in Figs. 4(a) and 4(b), respectively. At the low bias of 1 V, both transistors exhibit similar transfer characteristics with the *off* current of approximately 10^{-11} A. When increasing V_{SD} from 1 to 5 V, the current I_{SD} is enhanced by three orders in the transistor along the a axis. Moreover, the high leakage current appears in its *off* state again indicating the formation of a short channel. In contrast, the transistor in the 90° orientation does not show pronounced modulation by the application of V_{SD} within the *off* state. The leakage current is mostly maintained at the low value of approximately 10^{-11} A even at the high bias of 5 V.

The scenario is presented as illustrated in Figs. 4(c) and 4(d). At the low bias of 1 V, the Schottky barriers in both transistors are quite thick. No tunneling is possible even with the light carriers in the a axis. In fact, at the low dc bias regime, the tunneling transport is mostly prevented by the thick Schottky barrier in any orientations, making the extraction of the anisotropy information impossible (Fig. S4 within the Supplemental Material [22]). By increasing V_{SD} , the barriers are eventually thinned down. The light carriers along the a axis can tunnel through the Schottky barrier even at the *off* state, leading to the high leakage current as a short channel transistor. Although a consistent barrier is set under the same condition, it is less transparent for the much heavier carriers in the orientation of 90° . Consequently, tunneling is not activated along $\perp a$ such that low conductivity in the *off* state is

maintained and conductivity ratio to $\parallel a$ is colossal. Under such circumstance, tunneling can be enabled by applying additional gate voltage, which further narrows down the barrier as indicated in Fig. 4(d). The drain bias modulation can be observed in the junction *on* state. Hence, the conductivity ratio between $\parallel a$ and $\perp a$ is reduced in the *on* state. We plot the measurements along 30° orientation, where the DIBL effect is intermediate between 0° and 90° orientations (Fig. S5 within the Supplemental Material [22]).

III. CONCLUSION

In conclusion, we obtain the anisotropy of effective mass in ReSe₂, which is directly extracted from tunneling dominated Schottky transistors. The results reveal that ReSe₂ has heavy holes and electrons in the orientation normal to its a axis, resulting in the excellent immunity to DIBL effect for realizing field-effect transistors with very scaled-down channels. In contrast, the light carriers are measured along the a axis, which make ReSe₂ favorable for building tunneling devices, such as tunnel junctions or tunnel FET. The accuracy of this method is highlighted by comparing with ARPES data. This strategy provides a universal approach for all 2D semiconducting materials to widely and deeply investigate their anisotropic band properties at the lowest energy point. Furthermore, this anisotropic distribution of effective mass leads to an extremely high conductivity anisotropy of 10^3 , offering the opportunity for designing multifunctional directional memories based on tunneling devices for real applications.

ACKNOWLEDGMENTS

This work is supported by National Natural Science Foundation of China (Grant No. 11804397) and Hunan Provincial Science and Technology Department (Grant No. 2019RS1006). Y.Y. thanks the support of by Natural Science Foundation of Hunan Province, China (Grant No. 2019JJ50789).

- [1] Y. Liu, T. Low, and P. P. Ruden, Mobility anisotropy in monolayer black phosphorus due to scattering by charged impurities, *Phys. Rev. B* **93**, 165402 (2016).
- [2] Y.-C. Lin, H.-P. Komsa, C.-H. Yeh, T. Björkman, Z.-Y. Liang, C.-H. Ho, Y.-S. Huang, P.-W. Chiu, A. V. Krasheninnikov, and K. Suenaga, Single-layer ReS_2 : Two-dimensional semiconductor with tunable in-plane anisotropy, *ACS Nano* **9**, 11249 (2015).
- [3] H.-X. Zhong, S. Gao, J.-J. Shi, and L. Yang, Quasiparticle band gaps, excitonic effects, and anisotropic optical properties of the monolayer distorted 1T diamond-chain structures ReS_2 and ReSe_2 , *Phys. Rev. B* **92**, 115438 (2015).
- [4] Y. Yang, S.-C. Liu, X. Wang, Z. Li, Y. Zhang, G. Zhang, D.-J. Xue, and J.-S. Hu, Polarization-sensitive ultraviolet photodetection of anisotropic 2D GeS_2 , *Adv. Funct. Mater.* **29**, 1900411 (2019).
- [5] E. Zhang *et al.*, Tunable ambipolar polarization-sensitive photodetectors based on high-anisotropy ReSe_2 nanosheets, *ACS Nano* **10**, 8067 (2016).
- [6] X. Feng, X. Huang, L. Chen, W. C. Tan, L. Wang, and K.-W. Ang, High mobility anisotropic black phosphorus nanoribbon field-effect transistor, *Adv. Funct. Mater.* **28**, 1801524 (2018).
- [7] J. P. Echeverry and I. C. Gerber, Theoretical investigations of the anisotropic optical properties of distorted 1T ReS_2 and ReSe_2 monolayers, bilayers, and in the bulk limit, *Phys. Rev. B* **97**, 075123 (2018).
- [8] N. R. Pradhan, C. Garcia, B. Isenberg, D. Rhodes, S. Feng, S. Memaran, Yan Xin, Amber McCreary, Angela R. Hight Walker, A. Raeliarjaona, H. Terrones, M. Terrones, S. McGill, and L. Balicas, Phase modulators based on high mobility ambipolar ReSe_2 field-effect transistors, *Sci. Rep.* **8**, 12745 (2018).
- [9] C. Kim, I. Moon, D. Lee, M. S. Choi, F. Ahmed, S. Nam, Y. Cho, H.-J. Shin, S. Park, and W. J. Yoo, Fermi level pinning at electrical metal contacts of monolayer molybdenum dichalcogenides, *ACS Nano* **11**, 1588 (2017).
- [10] A. Arora, J. Noky, M. Drüppel, B. Jariwala, T. Deilmann, R. Schneider, R. Schmidt, O. Del Pozo-Zamudio, T. Stiehm, A. Bhattacharya, P. Krüger, S. M. de Vasconcellos, M. Rohlfing, and R. Bratschitsch, Highly anisotropic in-plane excitons in atomically thin and bulklike 1T- ReSe_2 , *Nano Lett.* **17**, 3202 (2017).
- [11] A. Surrente, A. A. Mitioglu, K. Galkowski, W. Tabis, D. K. Maude, and P. Plochocka, Excitons in atomically thin black phosphorus, *Phys. Rev. B* **93**, 121405(R) (2016).
- [12] E. Liu *et al.*, Integrated digital inverters based on two-dimensional anisotropic ReS_2 field-effect transistors, *Nat. Commun.* **6**, 6991 (2015).
- [13] B. S. Kim, W. S. Kyung, J. D. Denlinger, C. Kim, and S. R. Park, Strong one-dimensional characteristics of hole-carriers in ReS_2 and ReSe_2 , *Sci. Rep.* **9**, 2730 (2019).
- [14] W. Jin, P.-C. Yeh, N. Zaki, D. Zhang, J. T. Sadowski, A. Al-Mahboob, A. M. van der Zande, D. A. Chenet, J. I. Dadap, I. P. Herman, P. Sutter, J. Hone, and R. M. Osgood, Jr., Direct Measurement of the Thickness-Dependent Electronic Band Structure of MoS_2 Using Angle-Resolved Photoemission Spectroscopy, *Phys. Rev. Lett.* **111**, 106801 (2013).
- [15] Y. Yuan, X. Wang, J. Kosel, and J. Sun, Quantum oscillations on the surface of InAs epilayer, *Phys. E: Low-Dimens. Syst. Nanostruct.* **114**, 113604 (2019).
- [16] A. V. Penumatcha, R. B. Salazar, and J. Appenzeller, Analysing black phosphorus transistors using an analytic Schottky barrier MOSFET model, *Nat. Commun.* **6**, 8949 (2015).
- [17] X. Liu, D. Qu, J. Ryu, F. Ahmed, Z. Yang, D. Lee, and W. J. Yoo, P-type polar transition of chemically doped multilayer MoS_2 transistor, *Adv. Mater.* **28**, 2345 (2016).
- [18] T. Agarwal, G. Fiori, B. Soree, I. Radu, M. Heyns, and W. Dehaene, Towards high-performance polarity-controllable FETs with 2D materials, *IEEE J. Electron Dev.* **6**, 979 (2018).
- [19] S. Das, A. Prakash, R. Salazar, and J. Appenzeller, Toward low-power electronics: Tunneling phenomena in transition metal dichalcogenides, *ACS Nano* **8**, 1681 (2014).
- [20] H. Liu, A. T. Neal, and P. D. Ye, Channel length scaling of MoS_2 MOSFETs, *ACS Nano* **6**, 8563 (2012).
- [21] D. Wolverson, S. Crampin, A. S. Kazemi, A. Ilie, and S. J. Bending, Raman spectra of monolayer, few-layer, and bulk ReSe_2 : An anisotropic layered semiconductor, *ACS Nano* **8**, 11154 (2014).
- [22] See Supplemental Material <http://link.aps.org-supplemental/10.1103/PhysRevApplied.13.044056> for sample fabrication and experimental setup, measurements of an additional device, optimal contact set by thermal annealing, extraction of effective Schottky barrier height, measurements at low dc biases, measurements along 30° from the *a* axis.
- [23] Y. Liu, J. Guo, E. Zhu, L. Liao, S.-J. Lee, M. Ding, I. Shakir, V. Gambin, Y. Huang, and X. Duan, Approaching the Schottky–Mott limit in van der Waals metal–semiconductor junctions, *Nature* **557**, 696 (2018).
- [24] A. Allain, J. Kang, K. Banerjee, and A. Kis, Electrical contacts to two-dimensional semiconductors, *Nat. Mater.* **14**, 1195 (2015).
- [25] C. Marquez, N. Salazar, F. City, C. Navarro, G. Mirabelli, J. C. Galdon, R. Duffy, S. Navarro, P. K. Hurley, and F. Gamiz, Investigating the transient response of Schottky barrier back-gated MoS_2 transistors, *2D Mater.* **7**, 025040 (2020).
- [26] J.-K. Lee, S. Jung, J. Park, S.-W. Chung, J. S. Roh, S.-J. Hong, I. H. Cho, H.-I. Kwon, C. H. Park, B.-G. Park, and J.-H. Lee, Accurate analysis of conduction and resistive-switching mechanisms in double-layered resistive-switching memory devices, *Appl. Phys. Lett.* **101**, 103506 (2012).
- [27] G. Nazir, H. Kim, J. Kim, K. S. Kim, D. H. Shin, M. F. Khan, D. S. Lee, J. Y. Hwang, C. Hwang, J. Suh, J. Eom, and S. Jung, Ultimate limit in size and performance of WSe_2 vertical diodes, *Nat. Commun.* **9**, 5371 (2018).
- [28] H. Wang *et al.*, Gate tunable giant anisotropic resistance in ultra-thin GaTe, *Nat. Commun.* **10**, 2302 (2019).